2015 American Control Conference
Palmer House Hilton
July 1-3, 2015. Chicago, IL, USA

Adaptive Control of an Aircraft with Uncertain Nonminimum-Phase Dynamics

Ahmad Ansari and Dennis S. Bernstein

Abstract— **This paper investigates four control architectures that use adaptive control to follow step, ramp, and harmonic roll-angle commands for a linearized aircraft model with an unknown transition from minimum-phase to nonminimum-phase (NMP) dynamics. In particular, we consider retrospective cost adaptive control (RCAC) with 1) a command-feedforward control architecture; 2) an output-feedback control architecture; 3) a centralized control architecture that uses both command feedforward and output feedback; and 4) a decentralized control architecture that uses both command feedforward and output feedback. For baseline tests, we assume that the location of the NMP zero is known. The goal of this work is to improve the transient response and rate of convergence. Numerical testing shows that RCAC with the decentralized control architecture using command feedforward and output feedback gives the fastest convergence. Furthermore, resetting controller coefficients at the start of the transition improves the transient response.**

I. Introduction

In many applications, nonminimum-phase (NMP) zeros limit the robustness and achievable performance of fixed-gain feedback control laws [1], [2]. Within adaptive control, NMP zeros present an additional impediment due to the possibility that the adaptive controller may attempt to cancel the NMP zeros. Consequently, adaptive control laws typically assume full-state-feedback control, which implies the absence of transmission zeros, or invoke positive real conditions, which imply that the plant is minimum phase and has relative degree one. Adaptive control of plants with NMP zeros remains a challenging problem.

In recent work, retrospective cost adaptive control (RCAC) has been applied to NMP systems with known NMP zeros [3]. For systems with unknown NMP zeros, constrained optimization is used in [4] to prevent unstable pole-zero cancellation.

To further motivate research in adaptive control of NMP systems, the present paper revisits the aircraft example considered in [5]. In particular, we consider the lateral dynamics of a flight vehicle that undergoes a time-varying transition from minimum-phase (MP) to NMP dynamics. This scenario is motivated by the dynamics of a hypersonic vehicle with unknown thermal effects [6], [7].

The present paper extends the results of [5] in several ways. First, unlike [5], which considered a single servo feedback loop, the present paper considers four control architectures, namely, command feedforward (CFF), output feedback (OFB), centralized control using both CFF and OFB, and decentralized control using both CFF and OFB. For each architecture, we choose appropriate regressor signals while adapting on the roll-command error. In particular, the regressor signal for CFF is the roll-angle command, while the regressor signal for OFB is the roll-command error.

The CFF and OFB architectures have different properties. In CFF there is no instability risk, whereas OFB improves the transient response through stability augmentation. The centralized and decentralized architectures take advantage of CFF and OFB.

In addition to the four control architectures, the present paper considers three techniques for facilitating adaptive control during the transition from MP to NMP dynamics. Specifically, at the start of the transition we consider 1) resetting the controller coefficients to zero, 2) resetting the covariance to its initial value, and 3) reversing the signs of the controller coefficients.

Ahmad Ansari, and D. S. Bernstein are with the Department of Aerospace Engineering, University of Michigan, Ann Arbor, MI, USA. {ansahmad, dsbaero}@umich.edu

II. Aircraft Model

We consider the lateral dynamics of an aircraft with a time-varying transition to NMP dynamics. We call the MP asymptotically stable plant the *nominal* plant and the NMP asymptotically stable plant the *off-nominal* plant. Discretizing the nominal and off-nominal plants given in [5] with $T_{\mathrm{s}} = 0.1$ sec yields

$$A_{\mathrm{nom}} = \begin{bmatrix} 0.9553 & 0.0265 & -0.0934 & 0.0039 \\ -2.5210 & 0.9680 & 0.1310 & -0.0050 \\ 0.0551 & 0.0045 & 0.9708 & 0.0001 \\ -0.1282 & 0.0989 & -0.0369 & 1.0004 \end{bmatrix},$$

$$A_{\mathrm{off}} = \begin{bmatrix} 0.8482 & 0.0255 & -0.0900 & 0.0038 \\ -10.3212 & 0.8595 & 0.5152 & -0.0210 \\ 0.0186 & 0.0041 & 0.9723 & 0.0001 \\ -0.5304 & 0.0953 & -0.0239 & 0.9999 \end{bmatrix},$$

$$B_{\mathrm{nom}} = \begin{bmatrix} 0.0034 \\ 0.2492 \\ -0.0017 \\ 0.0126 \end{bmatrix}, \quad B_{\mathrm{off}} = \begin{bmatrix} 0.0036 \\ 0.2390 \\ -0.0061 \\ 0.0124 \end{bmatrix},$$

where the control input is the elevon deflection and $x = \begin{bmatrix} \beta & P & R & \phi_{\mathrm{roll}} \end{bmatrix}^{\mathrm{T}}$, that is, sideslip angle, roll rate, yaw rate, and roll angle.

The transition to NMP dynamics occurs at a constant rate in the sense that $(A_{\mathrm{nom}}, B_{\mathrm{nom}})$ varies linearly to $(A_{\mathrm{off}}, B_{\mathrm{off}})$. For the examples below, the transition begins at $t = 250$ sec, and the transition from the nominal dynamics to the off-nominal dynamics takes 10 sec. Fig. 1 shows that the aircraft lateral dynamics are pointwise asymptotically stable throughout the transition. Unless stated otherwise, we assume that the exact locations of the NMP zeros (if any) at each

time step are known.

We consider the command-following problem for the roll angle $\phi_{\text{roll}} = y_0 = [0 \quad 0 \quad 0 \quad 1]x$ and minimize the roll-command error $e \triangleq \phi_{\text{roll}} - r$, where r is the roll-angle command. Fig. 2 shows the absolute values of the zeros of the elevon-to-roll transfer function during the transition. It also shows that the two imaginary MP zeros diverge along the real axis and one becomes NMP at 252.4 sec.

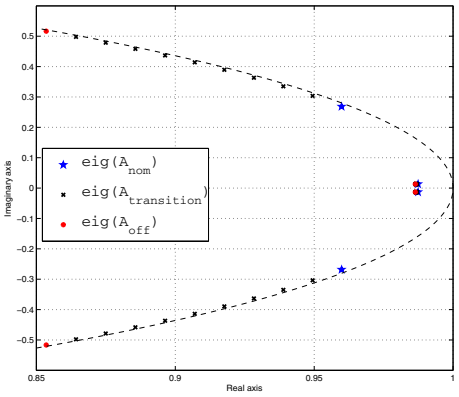

Fig. 1: Eigenvalue locations before, during, and after the transition from the nominal to the off-nominal plant. The lateral dynamics of the aircraft are pointwise asymptotically stable during the transition.

III. RCAC Formulation

Consider the MIMO discrete-time system

$$x(k+1) = Ax(k) + Bu(k) + D_1 w(k), \tag{1}$$

$$y(k) = Cx(k) + D_2 w(k), \tag{2}$$

$$z(k) = E_1 x(k) + E_0 w(k), \tag{3}$$

where $k \geq 0$, $x(k) \in \mathbb{R}^{l_x}$ is the state, $z(k) \in \mathbb{R}^{l_z}$ is the measured performance variable, $y(k) \in \mathbb{R}^{l_y}$ contains additional measurements that are available for control, $u(k) \in \mathbb{R}^{l_u}$ is the input, and $w(k) \in \mathbb{R}^{l_w}$ is the exogenous signal. The components of w can represent either the command signals to be followed, external disturbances to be rejected, or both, depending on the configurations of D_1 and E_0.

For command following, we choose w to be the roll-angle command r, and we construct D_1, E_1, and E_0 as

$$D_1 = 0, \qquad E_1 = \begin{bmatrix} 0 & 0 & 0 & 1 \end{bmatrix}, \quad E_0 = -1. \tag{4}$$

It follows that the performance variable z in (3) is the roll-command error e. C and D_2 are configured in various ways to obtain the control architectures discussed in Section IV.

The control-to-performance transfer matrix is defined by

$$G_{zu} \triangleq E_1(zI - A)^{-1}B. \tag{5}$$

Furthermore, for all $i \geq 1$, the i^{th} Markov parameter of G_{zu} is defined by

$$H_i \triangleq E_1 A^{i-1} B. \tag{6}$$

These parameters are used by RCAC.

The goal is to develop an adaptive output feedback controller that minimizes the performance variable z in the presence of the exogenous signal w with limited modeling information about (1)-(3). We consider the following formulation of RCAC given in [8], [9].

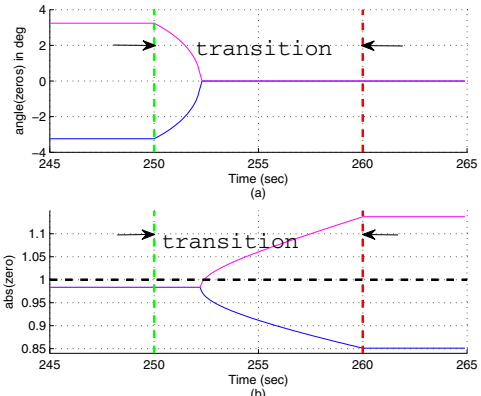

Fig. 2: (a) Angle of the zeros in the complex plane. (b) Zero magnitudes. The transition starts at 250 sec, and the two imaginary zeros become real at 252.4 sec. At the same time, one zero becomes NMP.

A. Control Law

We use the strictly proper time series control law

$$u(k) = \sum_{i=1}^{n_c} M_i^{\mathrm{T}}(k) u^{\mathrm{T}}(k-i) + \sum_{i=1}^{n_c} N_i^{\mathrm{T}}(k) y^{\mathrm{T}}(k-i), \tag{7}$$

where $M_i(k) \in \mathbb{R}^{l_u \times l_u}$ and $N_i(k) \in \mathbb{R}^{l_y \times l_u}$ are the controller coefficient matrices. The control law (7) can be reformulated as

$$u(k) = \Phi(k)\theta(k), \tag{8}$$

where $l_\theta = l_u n_c (l_u + l_y)$, and,

$$\theta(k) = \mathrm{vec}([M_1^{\mathrm{T}}(k) \cdots M_{n_c}^{\mathrm{T}}(k) \; N_1^{\mathrm{T}}(k) \cdots N_{n_c}^{\mathrm{T}}(k)]^{\mathrm{T}}), \in \mathbb{R}^{l_\theta}$$

$$\phi(k) = [u^{\mathrm{T}}(k-1) \cdots u^{\mathrm{T}}(k-n_c) \; y^{\mathrm{T}}(k-1) \cdots y^{\mathrm{T}}(k-n_c)]^{\mathrm{T}},$$

$$\Phi(k) = I_{lu} \otimes \phi^{\mathrm{T}}(k) \in \mathbb{R}^{l_u \times l_\theta}. \tag{9}$$

B. Retrospective Performance

Define $G_{\mathrm{f}}(\mathrm{q}) \triangleq D_{\mathrm{f}}^{-1}(\mathrm{q}) N_{\mathrm{f}}(\mathrm{q})$, where q is the forward shift operator, $n_{\mathrm{f}} \geq 1$ is the order of G_{f}, and

$$N_{\mathrm{f}}(\mathrm{q}) \triangleq K_1 \mathrm{q}^{n_{\mathrm{f}}-1} + K_2 \mathrm{q}^{n_{\mathrm{f}}-2} + \cdots + K_{n_{\mathrm{f}}}, \tag{10}$$

$$D_{\mathrm{f}}(\mathrm{q}) \triangleq I_{l_z} \mathrm{q}^{n_{\mathrm{f}}} + A_1 \mathrm{q}^{n_{\mathrm{f}}-1} + A_2 \mathrm{q}^{n_{\mathrm{f}}-2} + \cdots + A_{n_{\mathrm{f}}}. \tag{11}$$

Furthermore, $K_i \in \mathbb{R}^{l_z \times l_u}$ for $1 \leq i \leq r$, $A_j \in \mathbb{R}^{l_z \times l_z}$ for $1 \leq j \leq r$, and each polynomial $D_{\mathrm{f}}(\mathrm{q})$ is asymptotically stable. G_{f} can be chosen based on either Markov parameters of G_{zu}, or the nonminimum-phase zeros of G_{zu}. Next, for $k \geq 1$, we define the retrospective control as

$$\hat{u}(k) = \Phi(k)\hat{\theta}(k), \tag{12}$$

and the corresponding retrospective performance variable as

$$\hat{z}(\hat{\theta}(k), k) \triangleq z(k) + \Phi_{\mathrm{f}}(k)\hat{\theta}(k) - u_{\mathrm{f}}(k), \tag{13}$$

where

$$\Phi_{\mathrm{f}}(k) \triangleq G_{\mathrm{f}}(\mathrm{q})\Phi(k), \qquad u_{\mathrm{f}} \triangleq G_{\mathrm{f}}(\mathrm{q})u(k), \tag{14}$$

and $\hat{\theta}(k) \in \mathbb{R}^{l\theta}$ is determined by the optimization below.

In this paper, G_{f} is chosen to be an FIR filter.

C. Cumulative Cost and RCAC Update Law

For $k > 0$, we define the cumulative cost function

$$J(k, \hat{\theta}) \triangleq \sum_{i=k_0}^{k} \left(\hat{z}(i)^{\mathrm{T}} R_z \hat{z}(i) + [\Phi(i)\hat{\theta}]^{\mathrm{T}} R_u \Phi(i)\hat{\theta} \right)$$

$$+ [\hat{\theta} - \theta(0)]^{\mathrm{T}} R_\theta [\hat{\theta} - \theta(0)], \tag{15}$$

where R_θ, R_z, and R_u are positive definite.

Let $P(0) = R_\theta^{-1}$ and $\theta(0) = \theta_0$. Then, for all $k \geq 1$, the cumulative cost function (15) has a unique global minimizer $\theta(k)$ given by the RLS update

$$\theta(k) = \theta(k-1) - P(k-1)\tilde{\Phi}(k)^{\mathrm{T}}\Gamma(k)^{-1} \cdot [\tilde{\Phi}(k)\theta(k-1) + \tilde{z}(k)], \tag{16}$$

where $P(k)$ satisfies

$$\begin{aligned} P(k) &= P(k-1) - P(k-1)\tilde{\Phi}(k)^{\mathrm{T}}\Gamma(k)^{-1}\tilde{\Phi}(k)P(k-1), \\ \tilde{\Phi}(k) &\triangleq \begin{bmatrix} \Phi_{\mathrm{f}}(k) \\ \Phi(k) \end{bmatrix} \in \mathbb{R}^{(l_z+l_u)\times l_\theta}, \\ \tilde{R}(k) &\triangleq \begin{bmatrix} R_z(k) & 0 \\ 0 & R_u(k) \end{bmatrix} \in \mathbb{R}^{(l_z+l_u)\times(l_z+l_u)}, \\ \tilde{z}(k) &\triangleq \begin{bmatrix} z(k) - u_{\mathrm{f}}(k) \\ 0 \end{bmatrix} \in \mathbb{R}^{l_z+l_u}, \\ \Gamma(k) &\triangleq \tilde{R}(k)^{-1} + \tilde{\Phi}(k)P(k-1)\tilde{\Phi}(k)^{\mathrm{T}}. \end{aligned} \tag{17}$$

IV. CONTROL ARCHITECTURE

By suitably choosing C and D_2 in (2), RCAC can accommodate various control architectures. Moreover, RCAC gives SISO or MIMO controllers depending on the dimensions of u and y in (1) and (2), respectively. We use this functionality to investigate the following control architectures for command following. For all control architectures, the goal is to follow step, ramp, and harmonic roll-angle commands r.

A. Command Feedforward (CFF)

Since the nominal and off-nominal plants are asymptotically stable (see Fig. 1), CFF can be used. For this architecture, we configure C and D_2 such that y in (2) is the roll-angle command r, that is,

$$C = [0 \quad 0 \quad 0 \quad 0], \qquad D_2 = 1. \tag{18}$$

Thus the components of Φ in (9) include the roll-angle command r and the input u. Fig. 3 shows that RCAC updates

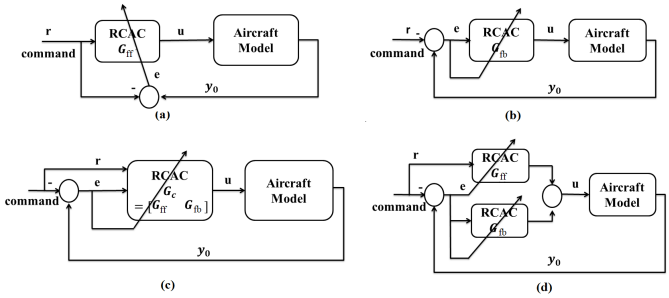

Fig. 3: Control architectures. (a) Command feedforward (b) Output feedback (c) Centralized command-feedforward with output-feedback (d) Decentralized command-feedforward with output-feedback

G_{ff} at each time step in order to follow step, ramp, and harmonic commands.

B. Output Feedback (OFB)

The output-feedback architecture can provide command following with stability augmentation. This architecture corresponds to

$$C = [0 \quad 0 \quad 0 \quad 1], \qquad D_2 = -1. \tag{19}$$

Thus the components of Φ in (9) include the roll-command error e and the input u. Fig. 3 shows the OFB architecture. The advantage of this architecture is that the closed-loop can provide stability augmentation.

C. Centralized Command-Feedforward with Output-Feedback (CFFOFB/C)

For this architecture, we choose

$$C = \begin{bmatrix} 0 & 0 & 0 & 1 \\ 0 & 0 & 0 & 0 \end{bmatrix}, \qquad D_2 = \begin{bmatrix} -1 \\ 1 \end{bmatrix}, \tag{20}$$

so that,

$$y = \begin{bmatrix} e \\ r \end{bmatrix}. \tag{21}$$

Thus the components of Φ in (9) include the roll-command error e, roll-angle command r, and the input u. Fig. 3 shows the CFFOFB/C architecture. Note that there is a single RCAC block that updates both G_{ff} and G_{fb} at each time step.

D. Decentralized Command-Feedforward with Output-Feedback (CFFOFB/D)

For this architecture we use two separate RCAC blocks, one for CFF and the other for OFB as shown in Fig. 3. We configure C and D_2 for CFF and OFB blocks as in (18) and (19), respectively. The advantage of this architecture is that we can tune both blocks separately by choosing different RCAC parameters for G_{ff} and G_{fb}.

V. METHODS FOR IMPROVING THE TRANSIENT RESPONSE

The results in [5] show that with NMP zero information, RCAC can follow the command with an undershoot of 9.7 deg at the transition from MP to NMP dynamics. Fig. 4 shows that the controller coefficients θ change during the transition and converge to new values with opposite signs. Noticing this trend, we consider the following methods for improving the transient response:

- M1 Reset $\theta(k)$ in (16) to zero at the start of the transition from MP to NMP elevon-to-roll dynamics.
- M2 Reset $P(k)$ in (17) to $P(0)$ at the start of the transition from MP to NMP elevon-to-roll dynamics.
- M3 Reverse the sign of $\theta(k)$ in (16) at the start of the transition from MP to NMP elevon-to-roll dynamics.

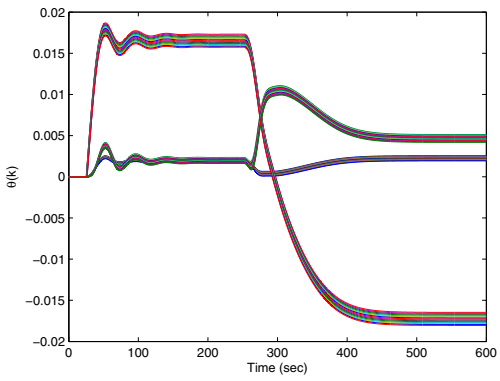

Fig. 4: Step command following with NMP zero information. At the transition, the controller coefficients readapt and converge to new values in the opposite direction relative to zero.

VI. Command Feedforward (CFF)

We construct Φ using the roll-angle command r. We choose $n_c = 1, R_\theta = 1.1I_{l_\theta}, R_z = 1, R_u = 0$, and $G_{\rm f} = 1$ for MP and -1 for NMP. RCAC updates the first-order feedforward controller $G_{\rm ff}(z) = \frac{\theta_2(k)}{z+\theta_1(k)}$ and is able to follow step and ramp commands (see Figs. 5-6). For harmonic commands, the controller order n_c needs to be at least 2 in order to shift the phase of the command. Fig. 7 shows that increasing the controller order gives faster convergence of the controller coefficients θ. Furthermore, after the transition from MP to NMP dynamics, numerical tests in Section V show that RCAC is able to follow the harmonic command using either M1 or M3. Fig. 8 shows harmonic command following using CFF.

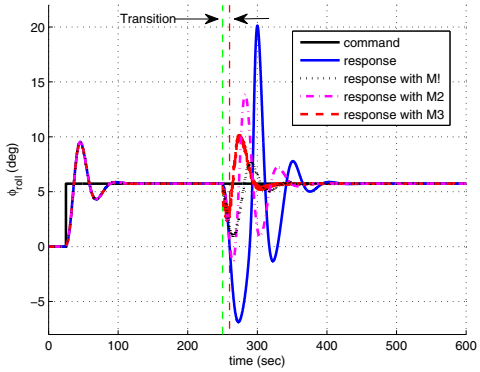

Fig. 5: CFF with a step command. By using M1, M2 or M3, RCAC follows the command with improved transient response during the transition.

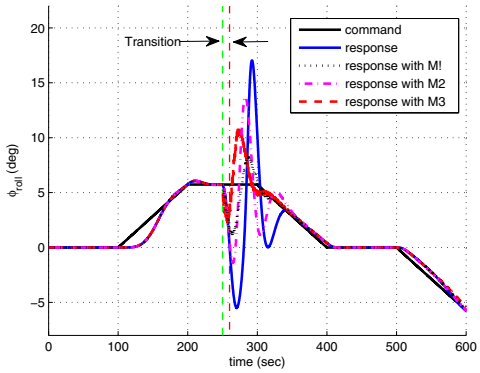

Fig. 6: CFF with a trapezoidal command. By using M1, M2 or M3, RCAC follows the command with improved transient response during the transition.

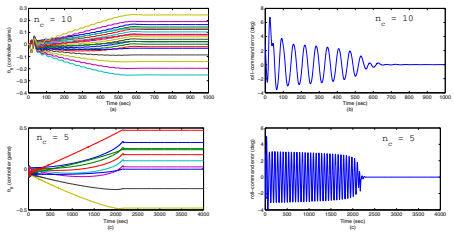

Fig. 7: CFF of the off-nominal plant with $r(k) = \sin(0.1k)$. Faster convergence is noticed with relatively larger controller order.

VII. Output Feedback (OFB)

For OFB we construct Φ using the roll-command error e. We choose $n_c = 15, R_\theta = 1.1I_{l_\theta}, R_z = 1$, and $R_u = 10^{-3}$. We construct $G_{\rm f}$ such that the coefficients

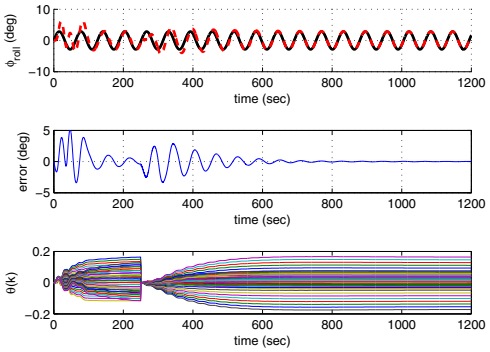

Fig. 8: CFF with the harmonic command $r(k) = \sin(0.1k)$. By resetting θ to zero at the start of the transition, RCAC follows the command after the transition from MP to NMP elevon-to-roll dynamics.

$K_1, \ldots, K_{\rm nf}$ are equivalent to $H_1 \times poly(NMPzeros)$, where $poly(NMPzeros)$ is a polynomial whose roots are the NMP zeros. If there are no NMP zeros, then $poly(NMP) = 1$. Fig. 9 shows that RCAC is able to follow step commands. However, the response is slower than CFF, and the roll-angle command error does not converge to zero. In addition, using M1 or M3 improves the transient response without degrading the steady-state error. Similar behavior is observed with ramp and harmonic commands.

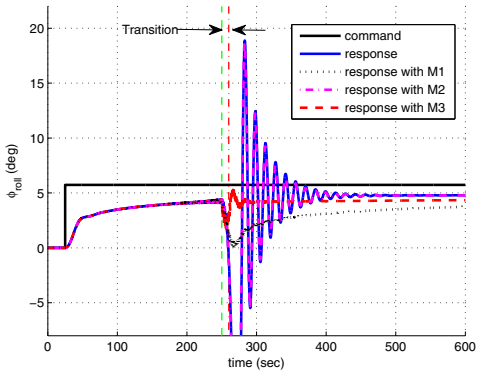

Fig. 9: OFB with a step command. RCAC follows the command with an asymptotic offset.

VIII. Centralized Command-Feedforward with Output-Feedback (CFFOFB/C)

We construct Φ with the roll-angle command r and the roll-command error e. As in Section IV-C, RCAC uses features of both CFF and OFB. We choose $n_c = 15, R_\theta = 1.1I_{l_\theta}, R_z = 1$, and $R_u = 0$. We construct $G_{\rm f}$ as in Section VII. Figs. 10-12 show that RCAC follows step, ramp, and harmonic commands; however for harmonic commands the response is slower than CFF. Moreover, Figs. 10-12 show that M1, M2, and M3 improve the transient response during the transition from MP to NMP dynamics.

IX. Decentralized Command-Feedforward with Output-Feedback (CFFOFB/D)

In the decentralized architecture, we use separate SISO RCAC blocks for both CFF and OFB in order to control the roll response of the aircraft.

A. CFFOFB/D with $\phi_{\rm roll}$ as measurement

In this architecture, we combine CFF and OFB by using two SISO RCAC blocks. The corresponding Φ, $G_{\rm f}$, and all

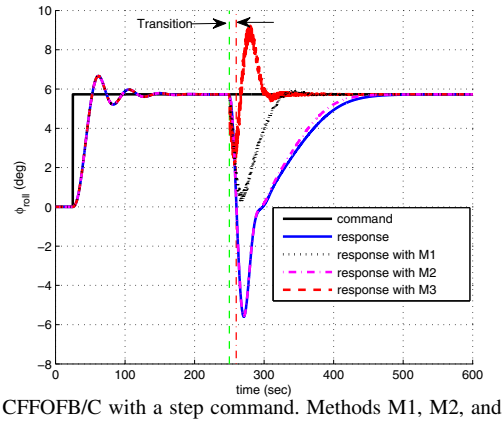

Fig. 10: CFFOFB/C with a step command. Methods M1, M2, and M3 give improved transient response and convergence.

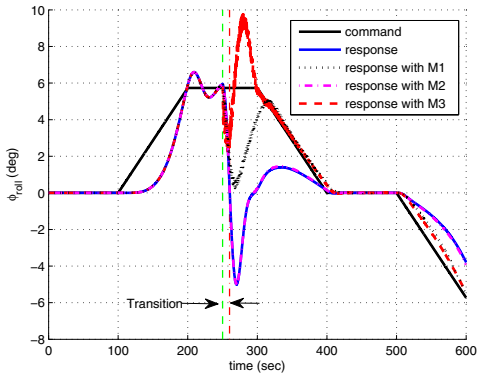

Fig. 11: CFFOFB/C with a trapezoidal command. By using M1, M2, and M3, RCAC follows the command with improved transient response during the transition.

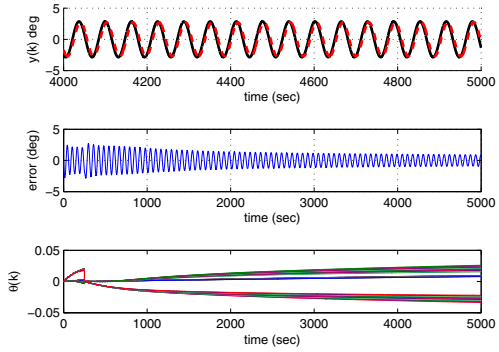

Fig. 12: CFFOFB/C with the harmonic command $r(k) = \sin(0.1k)$. By reversing the sign of θ at the start of the transition, RCAC is able to follow the command after the transition from MP to NMP elevon-to-roll dynamics. However, the response has a non-zero asymptotic error.

other RCAC parameters are the same as in Sections VI and VII. Figs. 13-15 show that RCAC is able to follow step, ramp, and harmonic commands.

B. CFFOFB/D with $\phi_{\rm roll}$ and $\dot{\phi}_{\rm roll}$

We use three SISO RCAC in this architecture. The two RCAC blocks are the same as in Section IX-A, while the third RCAC minimizes the roll rate $\dot{\phi}_{\rm roll}$. We construct the regressor Φ with the roll-command error e and choose $n_c = 10, R_\theta = 10^{-2} I_{l_\theta}, R_z = 1$, and $R_u = 0$. We construct $G_{\rm f}$ as in Section VII and apply M1 to improve the transient response. Fig. 16 shows that the roll rate in the feedback

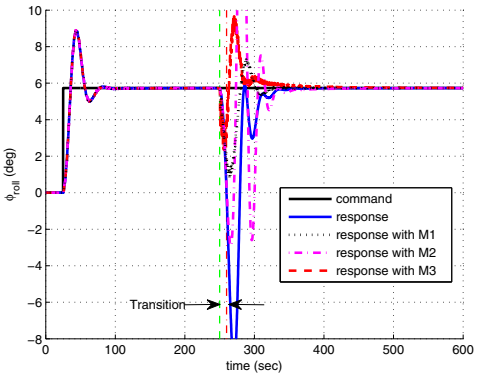

Fig. 13: CFFOFB/D with a step command (Section IX-A). Note that the methods M1 and M3 exhibit transients, with reduced response undershoot.

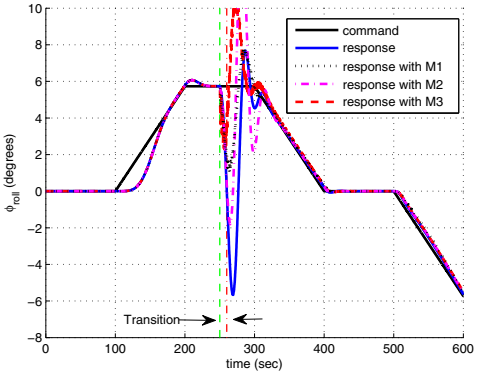

Fig. 14: CFFOFB/D with a trapezoidal command (Section IX-A). CFFOFB/D gives faster convergence than CFF and CFFOFB/C (see Figs. 6 and 11).

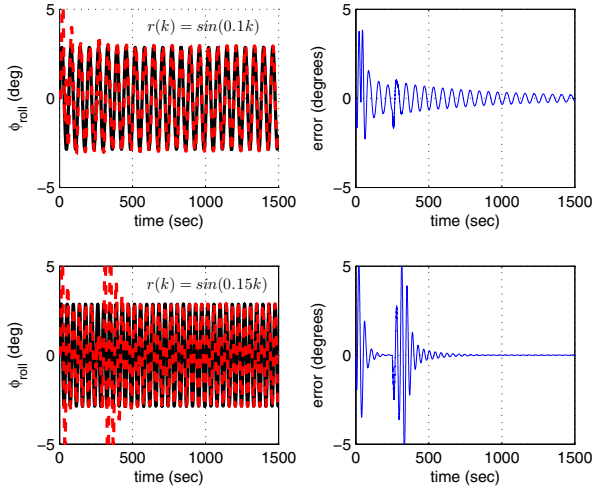

Fig. 15: Harmonic command following using CFFOFB/D (Section IX-A). By using method M1 or M3 in V, RCAC is able to follow the command after the transition from MP to NMP elevon-to-roll dynamics.

gives a slight improvement during the NMP dynamics. For the nominal plant, however, the step response deteriorates.

X. Uncertain Zeros at the Start, During, and After the Transition from MP to NMP Dynamics

We investigate a case with uncertain zeros at the start, during, and after the transition from MP to NMP dynamics. We assume that the transition onset time is known, and use

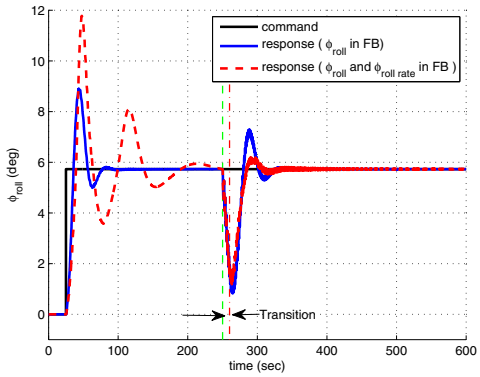

Fig. 16: CFFOFB/D with a step command (sections IX-A and IX-B). Using roll rate in the feedback gives a slight improvement during the NMP dynamics. For the nominal plant, however, the step response deteriorates.

CFFOFB/D as the control architecture. We define the uncertain zeros to be the zeros with a constant scaling factor. This implies that we over/underestimate the zeros of the elevon-to-roll transfer function by scaling them up/down. Fig. 17 shows that RCAC follows the roll-angle step command with 10% over/underestimation in the values of the zeros.

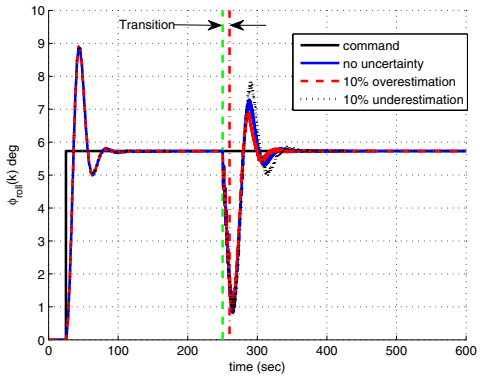

Fig. 17: CFFOFB/D with uncertain zeros. The zeros of the elevon-to-roll transfer function are uncertain at the start, during, and after the transition from MP to NMP dynamics. Note that RCAC is able to follow the step command with 10% over/underestimation in the values of the zeros.

XI. Summary of Results

We define settling time to be the time taken by the roll-angle response to reach 92% of the roll-angle command r. Table. I summarizes the results of the four control architectures. Based on the rate of convergence as the performance metric, the results show that the *decentralized command-feedforward with output-feedback* is the most promising control architecture for the given problem. However if the criterion is to avoid complexity, then the *command-feedforward control architecture* appears to be encouraging, as it needs a lower controller order, and uses knowledge of only the transition onset time.

XII. Conclusion

In this paper, four control architectures in the context of adaptive control were investigated. In this regard, we used retrospective cost adaptive control (RCAC) to illustrate all four control architectures in order to control the roll response of an aircraft with a transition from MP to NMP dynamics. We showed that, under the assumption that the NMP zero

TABLE I: summary of the step roll-angle command response

Architecture	**Controller order** n_c	**Exact Knowledge of NMP zero locations at each** T_s	**Knowledge of the transition onset time**	**Settling Time for Step command** (sec)
CFF	1	not used	used	358.92
OFB	10	used	not used	335.66
CFFOFB/C	15	used	not used	384.01
CFFOFB/D (with $\phi_{\rm roll}$)	CFF=1 OFB=10	used	not used	304.64

locations are available at each T_s, RCAC was able to follow step, ramp, and harmonic commands. Furthermore, in the feedforward case, we showed that RCAC used the transition onset time only, and was able to follow step, ramp, and harmonic commands. We showed that all of the control architectures converge to different controller coefficients, before and after the transition from MP to NMP dynamics. To improve the transient response, we considered various scenarios for implementing RCAC during the transition. Numerical testing showed that, if decentralized command-feedforward with output-feedback control architecture is used with resetting controller coefficients at the start of the transition, faster convergence with improved transient response is obtained compared to the other control architectures.

References

[1] J. Yan, J. B. Hoagg, R. E. Hindman, and D. S. Bernstein, "Longitudinal Aircraft Dynamics and the Instantaneous Acceleration Center of Rotation: The Case of the Vanishing Zeros," *IEEE Contr. Sys. Mag.*, vol. 30, pp. 68–92, 2011.

[2] J. B. Hoagg and D. S. Bernstein, "Nonminimum-Phase Zeros: Much to Do about Nothing," *IEEE Contr. Sys. Mag.*, vol. 27, no. June, pp. 45–57, 2007.

[3] J. B. Hoagg and D. Bernstein, "Retrospective Cost Model Reference Adaptive Control for Nonminimum-Phase Systems," *AIAA J. Guid. Contr. Dyn.*, vol. 35, pp. 1767–1786, 2012.

[4] A. Morozov, A. M. D'Amato, J. B. Hoagg, and D. S. Bernstein, "Retrospective cost adaptive control for nonminimum-phase systems with uncertain nonminimum-phase zeros using convex optimization," in *Proc. Amer. Contr. Conf.*, June 2011, pp. 1188–1193.

[5] Y. Rahman, K. Aljanaideh, E. D. Sumer, and D. S. Bernstein, "Adaptive control of aircraft lateral motion with an unknown transition to nonminimum-phase dynamics," *Proc. ACC*, pp. 2359–2364, 2014.

[6] M. A. Bolender and D. B. Doman, "Flight path angle dynamics of airbreathing hypersonic vehicles," in *Proc. AIAA Guid. Nav. Contr. Conf.*, Keystone, CO, August 2006, aIAA-2006-6692.

[7] B. Xu, D. Wang, F. Sun, and Z. Shi, "Direct neural control of hypersonic flight vehicles with prediction model in discrete time," *Neurocomputing*, vol. 115, pp. 39–48, 2013.

[8] E. D. Sumer, A. M. D'Amato, A. M. Morozov, J. B. Hoagg, and D. S. Bernstein, "Robustness of retrospective cost adaptive control to markov-parameter uncertainty," in *Proc. Conf. Dec. Contr.*, Orlando, FL, December 2011, pp. 6085–6090.

[9] E. D. Sumer and D. S. Bernstein, "Retrospective cost adaptive control with error-dependent regularization for mimo systems with uncertain nonminimum-phase transmission zeros," in *Proc. AIAA Guid. Nav. Contr. Conf.*, Minneapolis, MN, August 2012, aIAA-2012-4670-123.